Journal of Alloys and Compounds 511 (2012) 9–13

Contents lists available at SciVerse ScienceDirect

Journal of Alloys and Compounds

journal homepage: www.elsevier.com/locate/jallcom

Ab initio lattice dynamics of Ni_2MnX (X = Sn, Sb) magnetic shape memory alloys

Savaş Ağduk, Gökhan Gökoğlu*

Department of Physics, Karabük University, 78050 Karabük, Turkey

ARTICLE INFO

Article history:
Received 30 June 2011
Received in revised form 27 August 2011
Accepted 29 August 2011
Available online 7 September 2011

Keywords:
Magnetically ordered materials
Elasticity
Phonons
Computer simulations

ABSTRACT

In this study, we present the results of first principles calculations of elastic constants and phonon properties of nickel–manganese based magnetic shape memory compounds Ni_2MnSn and Ni_2MnSb in stoichiometric composition. The plane wave basis sets and pseudopotential method within spin-polarized generalized gradient approximation (σ-GGA) scheme of the density functional theory is applied. In investigation of the phonon dispersion spectra, linear response technique of the Density Functional Perturbation Theory is used. Phonon softening is observed in dispersion spectra at the transverse acoustic mode (TA_2) in [$\zeta\,\zeta\,0$] direction as an indication of the structural instability of these systems to shear deformation. The vibrational instability of Ni_2MnSb system is larger than that of Ni_2MnSn yielding negative phonon frequencies. This vibrational anomaly is also verified by the low shear modulus and large elastic anisotropy ratio. The minority spin Fermi surfaces of both systems exhibit strong nesting features.

1. Introduction

Ferromagnetic shape memory (FMSM) systems exhibit extraordinary magneto-elastic properties and are possible candidates for applications in high technology devices. FMSMs are characterized by strong magneto-elastic coupling which results in structural phase transitions between different martensitic variants driven by external magnetic field instead of mechanical stress. As a prerequisite, the martensitic transformation temperature should be lower than the Curie temperature of the ferromagnetic phase under study. Some materials display striking structural responses to applied magnetic fields, undergoing either magnetic twin reorientation or field-induced phase transformations that lead to a macroscopic shape memory effect [1]. The certain full- and half-Heusler alloys, the ternary intermetallic compounds with general formula X_2YZ and XYZ, respectively, are good examples for these kinds of materials. In previous theoretical and experimental studies [2,3], it is reported that the Ni_2MnGa shape memory system shows strains up to 9.5% under a magnetic field less than 1 T.

The underlying physics behind martensitic phase transformations can be explained by softening of some phonon modes and related elastic stiffness coefficients. The most interesting phenomena observed in Ni–Mn based MSM systems is a vibrational anomaly in phonon dispersion curve, especially in low energy transverse acoustic mode (TA_2) of [$\zeta\,\zeta\,0$] direction [4–6]. This behavior has been approved by both inelastic neutron scattering experiments and first-principles calculations. The degree of softening in acoustic TA_2 mode depends on the temperature of the system according to Fermi surface nesting. A complete softening with negative frequencies in TA_2 branch of [$\zeta\,\zeta\,0$] direction of Ni_2MnAl structure has been reported in previous theoretical studies [7,8]. The neutron scattering experiments on this system verify the softening in TA_2 mode between the wave vector $\zeta = 0.25$ and $\zeta = 0.4$, but the phonon frequencies remain finite at any wave vector even at the lowest temperatures [9]. The martensitic transformations occur in Ni–Mn–Al systems only at compositions near the ideal stoichiometry [10]. In another experimental study on Ni_2MnIn system [11], it is also emphasized that to avoid disorders (e.g., B2 structure) is important for optimum magnetic properties.

It has been observed experimentally that NiMnX (X = In, Sn, Sb) Heusler compounds display transformations between austenitic ferromagnetic structure and martensite phase [12]. The related properties make these systems possible candidates for FMSM applications. In this study, we investigate the elastic and lattice dynamics properties of Ni_2MnSn and Ni_2MnSb full-Heusler compounds using density functional theory (DFT) with GGA functionals and ultrasoft pseudopotentials. The vibrational properties are investigated in the framework of density functional perturbation theory (DFPT). DFPT gives an accuracy for acoustic properties at the level that is obtained previously for electronic structure. Although Ni–Mn–Ga and Ni–Mn–Al systems have been studied extensively in several works, there is a lack of first principles study on Ni_2MnX (X = Sn, Sb) shape memory systems in literature. To the best of our knowledge, this is the unique first principles linear response study investigating the vibrational properties of the related systems. The rest of the paper is organized as follows: the details of calculations

* Corresponding author. Tel.: +90 370 433 8374; fax: +90 370 433 8334.
E-mail address: ggokoglu@gmail.com (G. Gökoğlu).

0925-8388/$ – see front matter © 2011 Elsevier B.V. All rights reserved.
doi:10.1016/j.jallcom.2011.08.092

performed are presented in Section 2. We present the results of the first-principles calculations of elastic constants, phonon dispersion spectra, and Fermi surfaces in successive subsections of Section 3. Finally, a conclusion is presented in Section 4.

2. Computational method

The stoichiometric full-Heusler alloys are ternary intermetallics with a generic formula X_2YZ for the $L2_1$ phase ($Fm\bar{3}m$ space group, ♯225). X atom is a transition metal which stands on (0 0 0) and (1/2 1/2 1/2) Wyckoff crystallographic positions, while Y and Z are a magnetic transition metal and a III–V group element occupying the positions (1/4 1/4 1/4) and (3/4 3/4 3/4), respectively. The importance of these materials results from the ferromagnetic behavior, even though none of the atoms in the composition is ferromagnetic. All the calculations presented in this study have been performed using the PWscf code, distributed with the Quantum ESPRESSO package [13,14].

Generalized gradient approximation of the density functional theory is used to approximate exchange-correlation potential with Perdew–Burke–Ernzerhof parametrization [15]. The ultrasoft pseudopotentials are used in all the calculations in this study. In generation of the pseudopotentials, a scalar relativistic calculation scheme is followed including non-linear core correction. The valence states of the atoms considered are as follows; Ni: $3d^8\ 4s^2$, Mn: $3p^6\ 4s^2\ 3d^5$, Sn: $4d^{10}\ 5s^2\ 5p^2$, Sb: $4d^{10}\ 5s^2\ 5p^3$. Brillouin zone integration is performed with automatically generated $14\times14\times14$ k-point mesh, following the convention of Monkhorst and Pack [16], yielding 208 k-points centered at Γ-point. Wave-functions are expanded in plane wave basis sets up to a kinetic energy cut-off value of 50 Ry. This produces approximately 2220 plane waves. The convergence criteria for total energy is 1×10^{-10} Ry in self-consistent calculations. Methfessel-Paxton type smearing is applied on fermionic occupation function with $\sigma = 0.02$ Ry smearing parameter [17].

The elastic stiffness coefficients of the cubic crystals under study, C_{11}, C_{12}, and C_{44} are calculated using volume conserving (isochoric) strains. The use of isochoric strains enables us to eliminate first order terms in energy due to the initial hydrostatic pressure. The shear constant C_s is calculated via tetragonal distortion, while a monoclinic distortion is used to calculate C_{44}. The strain energies can be given as

$$E(\delta) = E(0) + 6C_sV\delta^2 + O(\delta^3), \quad (1)$$

$$E(\delta) = E(0) + 2C_{44}V\delta^2 + O(\delta^4) \quad (2)$$

for tetragonal (1) and monoclinic (2) distortions, respectively. $E(0)$ is the unstrained ground state energy of the system and V is its volume. C_{44} and C_s are obtained from the quadratic coefficients of Eqs. (1) and (2). Other elastic constants (C_{11} and C_{12}) are calculated using C_s and B. The details of the calculation procedure and strain tensors used have been explained in detail in Refs. [18,19].

The phonon dispersion spectra are constructed by using DFPT in the linear response approach [20–22], in which second order derivatives of the total energy are calculated to obtain dynamical matrix. DFPT allows us to examine vibrational properties of materials at a high accuracy level. Energy threshold value for convergence is 1×10^{-16} Ry in phonon calculations. The dynamical matrices are produced in a k-point grid of $4\times4\times4$ in irreducible wedge of the Brillouin zone. Then the full phonon dispersion spectra can be calculated from interatomic force constants by Fourier transform of dynamical matrices.

3. Results and discussion

3.1. Elasticity

The properties of the equilibrium structures of the compounds under study are investigated in view of the Vinet equation of states [23], which is found to be most accurate among the various equation of states formulations in a previous study [24]. The calculated total energies at 30 different volumes are fitted to equation of states in order to estimate equilibrium lattice constants, bulk modulus, and its first pressure derivative. The equation of states formulation connects the total energy of the system to its volume at a fixed temperature. The obtained asymptotic standard errors in fitting process are less than 0.1% which is an indication of the precision of the calculation. All the calculated quantities are given in Table 1 together with available experimental results and other theoretical studies. The experimental values of equilibrium lattice constants are available for Ni_2MnSn and Ni_2MnSb systems. The calculated values of the present study are in excellent agreement with the recent experimental results of Ref. [25]. In that sense, GGA functionals can be regarded as successful in simulation of these types of metallic structures.

Table 1
Calculated, experimental, and other theoretical values of lattice constant, magnetic moment, elastic stiffness constants, and elastic anisotropy ratio of stoichiometric Ni_2MnSn and Ni_2MnSb.

	Present	Experimental	Theoretical
Ni_2MnSn			
a (Å)	6.068	6.05[a],6.05[g]	6.022[c],5.92[d],6.06[e]
μ (μ_B)	4.20	4.05[a], 4.10[b], 4.18[g]	4.09[c], 3.86[d], 4.08[e],3.97[f]
B (GPa)	138.4		168.5[d],140[e]
B'	4.89		2.9[d]
C_s(GPa)	14.8		8[e]
C_{11} (GPa)	158.1		151[e]
C_{12} (GPa)	128.5		135[e]
C_{44} (GPa)	81.3		87[e]
$A = C_{44}/C_s$	5.49		11[e]
Ni_2MnSb			
a (Å)	6.051	6.00[h]	6.0[d]
μ (μ_B)	4.12		3.87[d]
B (GPa)	139.7		168.3[d]
B'	5.30		6.0[d]
C_s(GPa)	3.0		
C_{11} (GPa)	143.7		
C_{12} (GPa)	137.7		
C_{44} (GPa)	74.9		
$A = C_{44}/C_s$	24.97		

[a] Ref. [33].
[b] Ref. [34].
[c] Ref. [35].
[d] Ref. [36].
[e] Ref. [27].
[f] Ref. [37].
[g] Ref. [25].
[h] Ref. [38].

In Fig. 1, we display the calculated relative energies as a function of magnitude of the strain for monoclinic and tetragonal distortions for both Ni_2MnSn and Ni_2MnSb systems. $\delta = 0$ corresponds to the original $L2_1$ Heusler structure. The systems are fully relaxed after each distortion in order to reduce the forces on the atom to less than 1×10^{-5} Ry/a.u. The ionic minimization process is performed by Broyden–Fletcher–Goldfarb–Shanno (BFGS) algorithm [26]. The calculated values of strain energy coincide with the fitting curves of Eqs. (1) and (2). The calculated elastic constants of Ni_2MnSn are consistent with the FLAPW-GGA calculations of Ref. [27]. In literature, we are not aware of any experimental study investigating the elastic constants of the systems under consideration. Moreover, there is no theoretical calculation available for the elastic properties of Ni_2MnSb. The elastic anisotropy ratio $A = C_{44}/C_s$ is an important quantity and measures the stability of the system to shear deformation. The large anisotropy values indicate unstable crystal

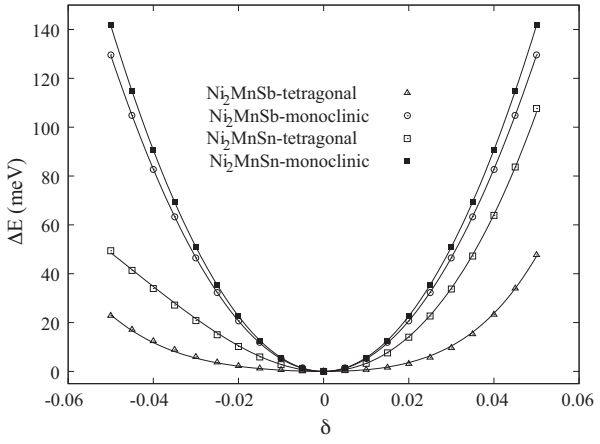

Fig. 1. Total energy as a function of strain magnitude together with fitting curves for tetragonal and monoclinic distortions.

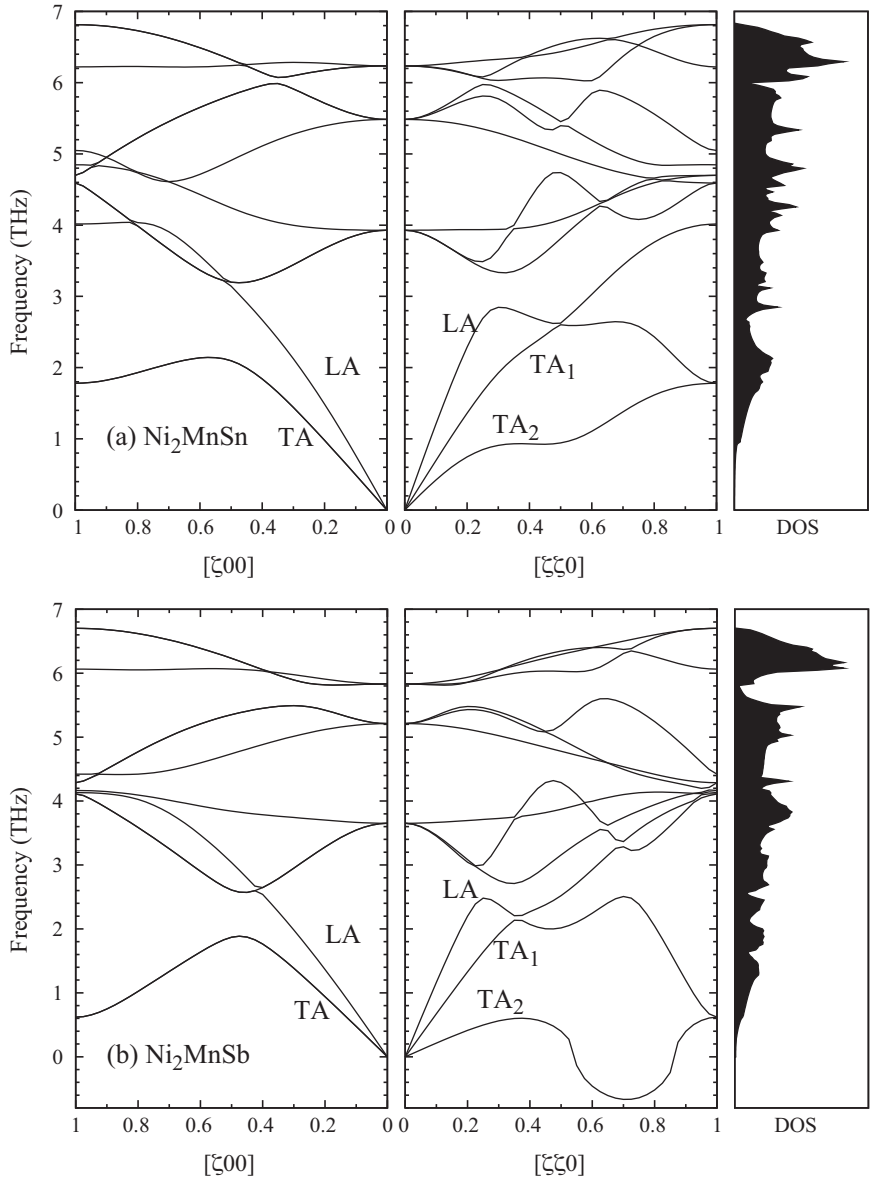

Fig. 2. The calculated, within linear response approach, phonon dispersion spectra of (a) Ni_2MnSn and (b) Ni_2MnSb systems. The horizontal scales of phonon dispersions are in units of $(2\pi/a)$. The total phonon densities of states are included at the right of phonon dispersions.

structures under stress across (1 1 0) plane. It is remarkable that the shear moduli (C_s) are very low for both systems. The calculated A values are 5.49 and 24.97 for Ni_2MnSn and Ni_2MnSb systems, respectively. These values are indications of structural instability of Ni_2MnSn and Ni_2MnSb single crystals. This situation is also a common property of the cubic crystals which exhibit martensitic phase transformations [28].

3.2. Lattice vibrations

The full phonon dispersion spectra are calculated within linear response approach of the density functional perturbation theory. The dynamical matrices are calculated at 8 **q**-vectors in irreducible Brillouin zone. Once interatomic force constants in real space are available, the dynamical matrix can be reconstructed at any desired value of **q**-vector [29]. In Fig. 2, we display the calculated phonon dispersion curves together with total vibrational density of states. To our knowledge, the phonon dispersions of the related compounds have not been reported previously. The transverse acoustical and optical branches in [1 0 0] direction are doubly degenerate due to the symmetry of cubic crystal, while the dispersion along [1 1 0] (Γ–K) direction is composed of non-degenerate 3 acoustical and 9 optical branches. The optical mode frequencies at Γ-point are 6.2, 5.5, and 3.9 THz for Ni_2MnSn and 5.8, 5.2, and 3.6 THz for Ni_2MnSb systems. These values are very close to each other for both systems studied. The vibrational frequencies of Ni_2MnSb are 0.3–0.4 THz lower than that of Ni_2MnSn according to the higher atomic mass of antimony compared to tin atom.

The most interesting phenomena observed in phonon dispersion curves is softening of acoustic TA_2 branches along $[\zeta\,\zeta\,0]$ directions for both systems. The softening occurs at $\zeta \approx 0.35$ and $\zeta \approx 0.40$ wave vectors for Ni_2MnSn and Ni_2MnSb, respectively. The softening of Ni_2MnSn system is relatively weak, so that the phonon frequencies remain finite at any wavevector along $[\zeta\,\zeta\,0]$. On the other hand, a remarkable vibrational instability is observed in TA_2 mode of Ni_2MnSb which consists of negative vibration frequencies between $\zeta = 0.55$ and $\zeta = 0.85$. These behaviors are also supported by the low shear moduli (C_s) and large elastic anisotropy ratio (A) of

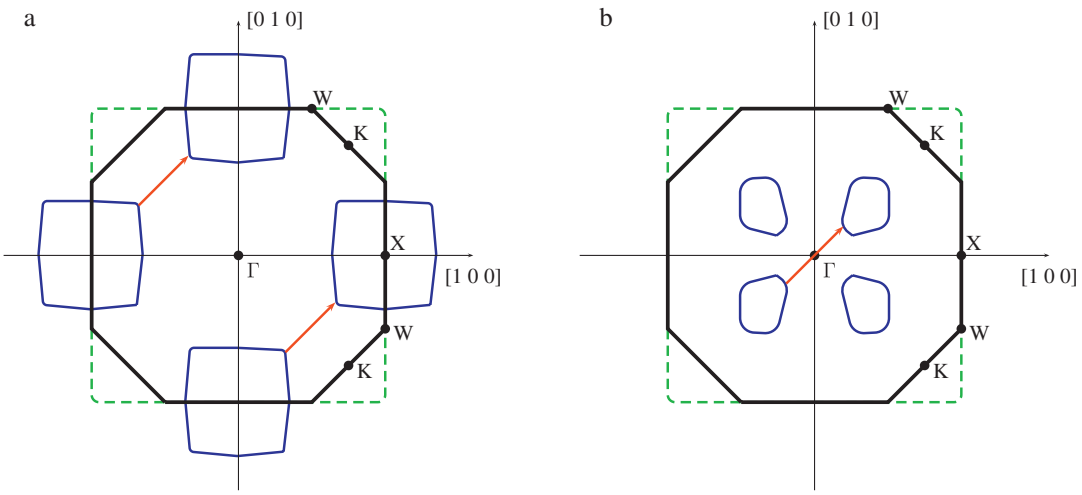

Fig. 3. 2D cross section of fcc Brillouin zone obtained by cutting from $k_z = 0$ plane for (a) Ni_2MnSn and (b) Ni_2MnSb. Black lines show the boundaries of BZ, blue lines indicate the electronic states. Red arrows are nesting vectors connecting adjacent electronic states within BZ. (For interpretation of the references to color in this figure legend, the reader is referred to the web version of the article.)

these systems as mentioned in Table 1. The large elastic anisotropy ratio of Ni_2MnSb ($A = 24.97$) results in negative vibrational modes in phonon spectra, since the elastic stiffness coefficients C_{44} and C_s are related to TA_1 and TA_2 branches along $[\zeta\,\zeta\,0]$ direction, respectively. These results indicate that the cubic $L2_1$ phase of Ni_2MnSn and Ni_2MnSb systems is unstable at low temperatures, since $L2_1$ structure is the high-temperature austenitic phase of these type of magnetic shape memory systems.

In a recent experimental study [30], the elastic properties and lattice dynamics of Ni_2MnIn shape memory system have been investigated by neutron scattering and ultrasonic techniques. A similar lattice instability in TA_2 branch of $[\zeta\,\zeta\,0]$ direction has been reported together with low shear modulus. It has also been emphasized that the softening deepens with decreasing temperature. The previous theoretical calculations on Ni_2MnX (X = Ga, Al, In, Ge) [4], Ni_2MnAl [8], Ni_2MnGa [31], and Ni_2MnIn [32] FMSM systems report softening at the same acoustic mode TA_2. In view of these studies and the results obtained, the observed anomaly can be ascribed to Kohn anomaly [31] and coupling of TA_2 mode to optical modes of Ni atoms [7].

The frequencies of lowest energy optical modes at Γ-point are 3.9 THz and 3.6 THz for Ni_2MnSn and Ni_2MnSb systems, respectively. These low energy modes have T_{2g} symmetry with Raman active nature, while the symmetry of other modes at Γ is T_{1u} with infrared-active vibrations. Two important point should be emphasized about the modes with T_{2g} symmetry at Γ. First of all, the energy of these vibrations is relatively low compared to the stable structures. Secondly, these are pure nickel vibrations standing on two different atomic positions without involving the vibrations of other atoms in composition. Consequently, the coupling of optical phonons with T_{2g} symmetry to the acoustical TA_2 vibrations contributes to the observed vibrational anomaly. In a previous theoretical study [4], it is suggested that the martensitic instability in Ni-based magnetic shape memory systems increases with increasing electron concentration. The e/a ratio is 7.745 and 7.930 for Ni_2MnSn and Ni_2MnSb, respectively. So that, the related argument of Ref. [4] is supported by the results presented in this study, since Ni_2MnSb shows larger softening compared to Ni_2MnSn.

3.3. Fermi surface nesting

Kohn anomaly in metallic systems is a result of the strong interaction of electronic states near Fermi level with phonons yielding a kink in phonon dispersion curves. This situation occurs at phonon wavevectors which are the nesting vectors of Fermi surface. In order to clarify these type of anomalous lattice vibrations, the detailed investigation of the nesting features of the Fermi surface can be useful. We have performed spin-polarized Fermi surface calculations by using much denser k-point mesh ($24 \times 24 \times 24$) in irreducible Brillouin zone. The minority spin Fermi surface structures present interesting nesting properties and give strong clues about the observed anomaly. In Fig. 3, the 2D Fermi surfaces of minority spin states obtained by cutting the Fermi surface at $k_z = 0$ plane are shown for Ni_2MnSn and Ni_2MnSb systems. As mentioned previously, the softening occurs at wavectors $\zeta \approx 0.35$ and $\zeta \approx 0.40$ along $[\zeta\,\zeta\,0]$ direction for Ni_2MnSn and Ni_2MnSb systems, respectively. The nesting vectors connecting the adjacent electronic states are $\mathbf{q} = 0.35(1, 1, 0)$ for Ni_2MnSn and $\mathbf{q} = 0.38(1, 1, 0)$ for Ni_2MnSb as shown in the figure. These are in great agreement with the phonon vectors in softening region as a confirmation of Kohn anomaly.

4. Conclusion

The elastic and phonon properties of Ni_2MnSn and Ni_2MnSb ferromagnetic shape memory systems are investigated from first principles density functional calculations. Phonon dispersion spectra are calculated by linear response approach of the density functional perturbation theory, while elastic stiffness constants are estimated by tetragonal and monoclinic strains. The lattice dynamics properties of the systems under study are reported for the first time. We observe phonon softening in acoustic TA_2 branch of both systems indicating lattice instability. Ni_2MnSb system exhibits larger instability than Ni_2MnSn with imaginary phonon frequencies along $[\zeta\,\zeta\,0]$ direction. The instability is also verified by the low shear elastic moduli and large elastic anisotropy ratio for both systems. It can be concluded that the cubic $L2_1$ structure is the high-temperature austenitic phase of Ni_2MnSn and Ni_2MnSb systems. The observed instabilities can be attributed to two major reasons. First one is the coupling of low energy optical mode (T_{2g}) at Γ-point to acoustic TA_2 vibrations, while the second one is a Kohn anomaly. Fermi surface analysis reveals that the Kohn anomaly is obvious with nesting features of the Fermi surface.

Acknowledgements

This research was supported in part by TÜBİTAK (The Scientific & Technological Research Council of Turkey) through TR-Grid e-Infrastructure Project, part of the calculations have been carried out at ULAKBİM Computer Center.

References

[1] S.O. Kart, T. Çağın, J. Alloy Compd. 508 (2010) 177.
[2] K. Ullakko, J.K. Huang, C. Kanter, R.C. O'Handley, V.V. Kokarin, Appl. Phys. Lett. 69 (1996) 1966.
[3] A. Sozinov, A.A. Likhachev, N. Lanska, K. Ullakko, Appl. Phys. Lett. 80 (2002) 1746.
[4] A.T. Zayak, P. Entel, K.M. Rabe, W.A. Adeagbo, M. Acet, Phys. Rev. B 72 (2005) 054113.
[5] Y. Lee, J.Y. Rhee, B.N. Harman, Phys. Rev. B 66 (2002) 054424.
[6] A. Zheludev, S.M. Shapiro, P. Wochner, A. Shwartz, M. Wall, L.E. Tanner, Phys. Rev. B 51 (1995) 11310.
[7] P. Entel, V.D. Buchelnikov, V.V. Khovailo, A.T. Zayak, W.A. Adeagbo, M.E. Gruner, H.C. Herper, E.F. Wassermann, J. Phys. D: Appl. Phys. 39 (2006) 865.
[8] T. Büsgen, J. Feydt, R. Hassdorf, S. Thienhaus, M. Moske, M. Boese, A. Zayak, P. Entel, Phys. Rev. B 70 (2004) 014111.
[9] X. Moya, L. Ma nosa, A. Planes, T. Krenke, M. Acet, V.O. Garlea, T.A. Lograsso, D.L. Schlagel, J.L. Zarestky, Phys. Rev. B 73 (2006) 064303.
[10] A. Morito, T. Kakeshita, K. Hirata, K. Otsuko, Acta Mater. 46 (1998) 5377.
[11] M. Kurfiß, F. Schultz, R. Anton, G. Meier, L. von Sawilski, J. Kötzler, J. Mag. Mag. Mater. 290–291 (2005) 591.
[12] Y. Sutou, Y. Imano, N. Koeda, T. Omori, R. Kainuma, K. Ishida, K. Oikawa, Appl. Phys. Lett. 85 (2004) 4358.
[13] Quantum-ESPRESSO is a community project for high-quality quantum-simulation software, based on density-functional theory, and coordinated by Paolo Giannozzi. See http://www.quantum-espresso.org and http://www.pwscf.org.
[14] P. Giannozzi, S. Baroni, N. Bonini, M. Calandra, R. Car, C. Cavazzoni, D. Ceresoli, G.L. Chiarotti, M. Cococcioni, I. Dabo, A. Dal Corso, S. Fabris, G. Fratesi, S. de Gironcoli, R. Gebauer, U. Gerstmann, C. Gougoussis, A. Kokalj, M. Lazzeri, L. Martin-Samos, N. Marzari, F. Mauri, R. Mazzarello, S. Paolini, A. Pasquarello, L. Paulatto, C. Sbraccia, S. Scandolo, G. Sclauzero, A.P. Seitsonen, A. Smogunov, P. Umari, R.M. Wentzcovitch, J. Phys.: Condens. Matter 21 (2009) 395502.
[15] J.P. Perdew, K. Burke, M. Ernzerhof, Phys. Rev. Lett. 77 (1996) 3865.
[16] H.J. Monkhorst, J.D. Pack, Phys. Rev. B 13 (1976) 5188.
[17] M. Methfessel, A.T. Paxton, Phys. Rev. B 40 (1989) 3616.
[18] G. Gökoğlu, A. Erkişi, Solid State Commun. 147 (2008) 221.
[19] G. Gökoğlu, J. Alloy Compd. 478 (2009) 653.
[20] X. Gonze, Phys. Rev. A 52 (1995) 1086.
[21] X. Gonze, Phys. Rev. A 52 (1995) 1096.
[22] S. Baroni, S. de Gironcoli, A.D. Corso, Rev. Mod. Phys. 73 (2001) 515.
[23] P. Vinet, J. Ferrante, J.R. Smith, J.H. Rose, J. Phys. C 19 (1986) L467.
[24] O. Gülseren, R.E. Cohen, Phys. Rev. B 65 (2002) 064103.
[25] Y. Chieda, T. Kanomata, K. Fukushima, K. Matsubayashi, Y. Uwatoko, R. Kainuma, K. Oikawa, K. Ishida, K. Obara, T. Shishido, J. Alloy Compd. 486 (2009) 51.
[26] H.B. Schlegel, J. Comput. Chem. 3 (1982) 214.
[27] A. Ayuela, J. Enkovaara, K. Ullakko, R.M. Nieminen, J. Phys.: Condens. Matter 11 (1999) 2017.
[28] A. Planes, L. Ma nosa, Solid State Phys. 55 (2001) 159.
[29] S. Baroni, S. de Gironcoli, A. Dal Corso, P. Giannozzi, Rev. Mod. Phys. 73 (2001) 515.
[30] X. Moya, D. González-Alonso, L. Ma nosa, A. Planes, V.O. Garlea, T.A. Lograsso, D.L. Schlagel, J.L. Zarestky, S. Aksoy, M. Acet, Phys. Rev. B 79 (2009) 214118.
[31] C. Bungaro, K.M. Rabe, A. Dal Corso, Phys. Rev. B 68 (2003) 134104.
[32] S. Ağduk, G. Gökoğlu, Eur. Phys. J. B 79 (2011) 509.
[33] P.J. Webster, Contemp. Phys. 10 (1969) 559.
[34] A. Deb, N. Hiraoka, M. Itou, Y. Sakurai, Phys. Rev. B 63 (2001) 205115.
[35] E. Şaşıoğlu, L.M. Sandratskii, P. Bruno, Phys. Rev. B 71 (2005) 214412.
[36] M. Pugaczowa-Michalska, Acta Physiol. Pol. A 113 (2008) 629.
[37] Y. Kurtulus, R. Dronskowski, G.D. Samolyuk, V.P. Antropov, Phys. Rev. B 71 (2005) 014425.
[38] P.J. Webster, K.R.A. Ziebeck, in: H.R.J. Wijn (Ed.), Alloys and Compounds of d-Elements with Main Group Elements, p. 2, Landolt-Börnstein, New Series, Group III, vol. 19/c, Springer, Berlin, 1988, pp. 75–184.